SYNTHESIS AND WAVELET ANALYSIS OF SIDE-SCAN SONAR SEA BOTTOM IMAGERY

JAROSŁAW TĘGOWSKI[1], ADAM ZIELINSKI[2]

[1]Institute of Oceanology, Polish Academy of Sciences,
Powstancow Warszawy 55, 81-712 Sopot, Poland
tegowski@iopan.gda.pl

[2]University of Victoria, Department of Electrical and Computer Engineering,
P.O. Box 3055, Victoria, BC V8W 3P6 Canada
adam@uvic.ca

A backscattered side-scan sonar signal contains indirect information about the scattering surface, namely, the bottom sediment, character of bottom surface, and seafloor relief. This paper presents a method of automatic estimation of height of seafloor characteristic objects and micro relief reconstruction applying the measured shadow length. The proposed method utilises coefficients of two-dimensional discrete wavelet decomposition of a side-scan sonar image as the input to the self-organised neural network classification algorithm. The heights of seafloor characteristic objects were the basis for synthesis of a three-dimensional map of the bottom surface. The computations were conducted for data recorded in Hornsund Fjord (Spitsbergen Island, Svalbard Archipelago) during a habitat mapping experiment and for synthetic data. The verification of the proposed algorithm was made by comparison of computed results with calibrated video recordings.

INTRODUCTION

The interpretation of seafloor maps produced by side-scan sonar is subject to consideration in many branches of sea exploration [1]. The raw information obtained from the sonar consists of a two-dimensional representation of the seafloor. However, three-dimensional information regarding height of obstacles, ripple marks, rocks, or objects of anthropogenic origin is crucial in many environmental studies. For instance, knowledge of seafloor ripple mark characteristics (e.g., height, width, shape regularity) is useful for current intensity measurement, turbulence parameter estimation, and sediment movement determination. The main advantage of side-scan sonar techniques compared to single and multi-beam acoustical techniques is the large spatial

resolution, on the order of centimetres. The main shortcoming of side-scan sonar imagery is that maps obtained this way are very dependant on sensor-to-scanned-object azimuth.

Conventional methods of seafloor characterisation are based on image texture analysis [2]. However, this type of analysis does not provide exact information about seafloor elevations and makes it necessary to search for methods that will enable bottom height determination. The intuitive approach depends on measurement of shadows produced by seafloor irregularities, which, combined with information about side-scan sonar fish altitude, can result in an elevation map. The numerous shape-from-shading approaches [3] can be divided into three computational techniques such as minimisation, propagation, and linearization. The first is based on minimisation of the energy function obtained from signals scattered at the whole ensonified area. Propagation approaches utilise generalization of height computations made for small areas, which can be related to the whole considered area. The last approach is based on information about bottom reflectivity contained in a backscattered signal. This method requires a calibrated side-scan sonar and, for that reason, most presented results are published using synthetic data [4]. Another problem in side-scan sonar imagery analysis is extraction of the object's shadow from the surrounding area. This question is especially important in military systems, where suitable image segmentation and classification enables mine hunting [5]. Template models [6] and fuzzy logic and statistical models [7] base shadow extraction and provision of information about characteristics of seafloor objects on a shape-from-shading approach. In this paper, we present a novel method of side-scan sonar imagery segmentation that provides satisfying results for seafloor object characterisation, including ripple-marks and seafloor obstacles.

The main motivation for this work was the analysis of acoustical measurement results obtained during the habitat mapping experiment conducted in Arctic Hornsund Fjord (Spitsbergen Island, Svalbard Archipelago) in August-September 2005, where the spatial distribution and biomass of macrophytobentos and seafloor morphological forms were subjects of investigation. The acoustical measurements were made using single beam Simrad EK-500 echosounder operating at 120 kHz and EdgeTech DF-1000 side-scan sonar operating at 100 kHz and 500 kHz. Verification of acoustical measurements by underwater calibrated video recording and biological sampling was made by divers. Some example data from this experiment have been processed in this paper.

1. ESTIMATION OF OBJECT SHADOWS

A side-scan sonar registers the backscattered signals from rough seafloor at low grazing angles. The general principle of sonar operation requires that a sonar sensor be situated at an altitude not greater than 40% of true (horizontal) range. The geometry of shadow formation is presented in Fig.1, where H is altitude of sensor, R is the slant range, H_p is the obstacle or ripple mark height, θ_g is grazing angle, and S is slant range of shadow. Equations 1 and 2 quantify geometrical dependences between shadow length and obstacle height:

$$S \cong \frac{H_p \cdot R}{H - H_p}, \tag{1}$$

$$H_p \cong \frac{H \cdot S}{R + S}. \tag{2}$$

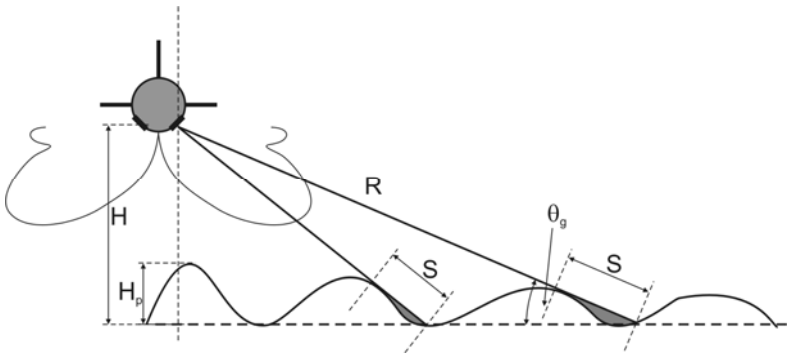

Fig.1 Scheme of shadow formation

The form of sonar imagery is strongly dependent on measurement geometry, which is determined by grazing angles of the incident signal. Fig. 2.a shows grazing angle as a function of true range changing from 1 m to 100 m and as altitude achieves 50 m. It should be noticed that for low grazing angles in case of long range or low sensor altitude, the extent of shadow will increase. Fig. 2.b shows shadow extent for fixed flight altitude of 10 meters and obstacles height 0.1 m, 0.5 m, 1.0 m, 1.5 m, and 2.0 m and horizontal distance to obstacles changing from 1 m to 100 m. For distance of 90 meters the shadow length is 10 times larger than the height of the obstacle. Accordingly, the acceptable shadow length requires the operation of a sonar sensor at adequate altitude.

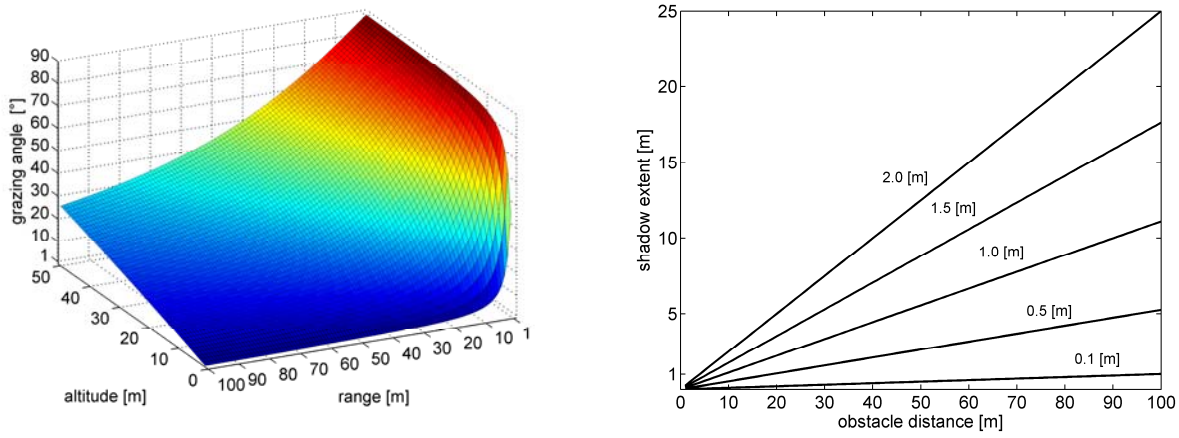

Fig.2 a) Grazing angle as the function of altitude of side-scan sonar flight and range of sonar beam, b) shadow extent for obstacles height changing from 0.1 m to 2 m and fixed flight height of 10 meters

The acoustical measurements in Hornsund Fjord area were conducted for variable sonar sensor altitude from 2 meters to 25 meters and variable slant ranges from 25 meters to 50 meters. Assumed ranges were derived from the depth range of the euphotic zone and experiment geometry (the side-scan sonars were set at a fixed depth of 2 m under the water surface). An example of seafloor image registered in Hornsund Fjord is shown in Fig. 3. The measurement area situated close to Wilczek Peninsula is known as a region of strong currents generated by tides and wind waves. These create ripple marks on the sandy bottom. The height of ripple marks does not exceed 0.4 m, verified by scaled underwater photography. The camera system was

attached to a tripod together with two lasers that produced two points at seafloor at a fixed distance. The inclination of camera lenses was established at 45^o. Geometrical dependencies of scaled photo images provided information about bottom obstacle sizes. The white rectangle shown in Fig.3 is an example area of ripple marks processed in this paper.

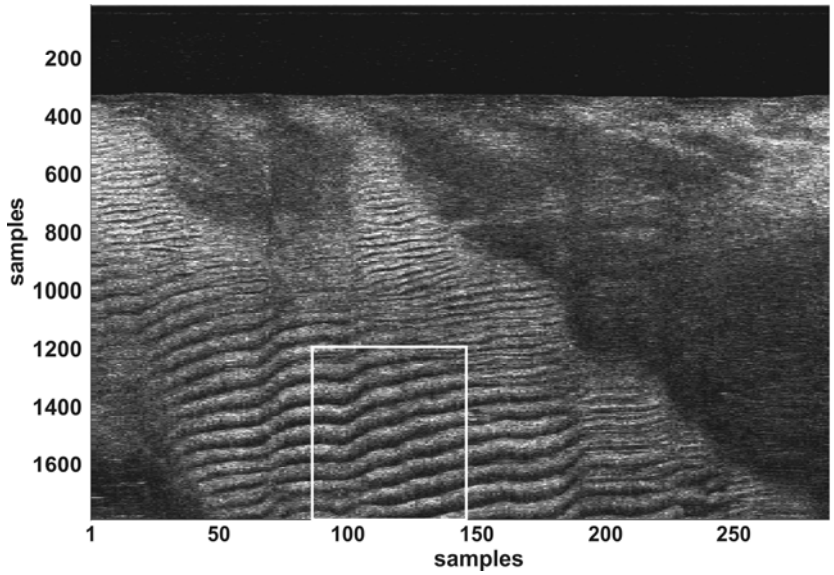

Fig.3 Example of ripple marks registered in Hornsund Fjord (Spitsbergen Island). The white rectangle marks the area considered in data processing algorithms

Processed sonar imagery was normalised by taking into consideration the following assumptions:

- loss of acoustical energy due to spreading and absorption;
- homogenous water layer;
- known altitude of the sonar sensor;
- the mean slope of the investigated area is 0^o (horizontal).

The loss of energy was compensated by a TVG function. The assumed constant sound speed provided the straight line geometry of sound propagation. The altitude of sonar sensor was estimated from the time of arrival of the first echo.

2. SONAR IMAGERY SEGMENTATION

The automatic determination of the height of seafloor surface forms is performed in three stages. In the first, the sonar imagery is subject to two-dimensional discrete wavelet decomposition. Next, the chosen coefficients of wavelet analysis are the input to a self-organised neural network algorithm or fuzzy logic clustering system, which produces image segmentation for two forms: bottom surface convexities (e.g., ripple marks) and shadows generated by these shapes. The third stage is an algorithm consisting of automatic, geometrical measurement of the length of each shadow (obtained as the result of the segmentation procedure), and computation of the height of each obstacle, ripple mark, or pebble using Equation 2.

The wavelet transform breaks the signal $S(x)$ into elements created by shifted and dilated versions of the basic function ψ (mother wavelet). The coefficients of the one-dimensional continuous wavelet transformation are given by:

$$W(a,b)=\int_{-\infty}^{+\infty} S(x)\frac{1}{\sqrt{a}}\psi\left(\frac{x-b}{a}\right)dx, \tag{3}$$

where a is a scale parameter controlling the function spread and b is a translation parameter - giving the spatial or time position of the scaled wavelet. In our computations, we chose the scales and positions based on powers of two-so-called dyadic scales, where $a=2^j$, $j\in Z$ and $b=ka$, $k\in Z$. The two-dimensional wavelet function can be described as:

$$\frac{1}{\sqrt{a_1 a_2}}\psi\left(\frac{x_1-b_1}{a_1},\frac{x_1-b_1}{a_1}\right),\quad x=(x_1,x_2)\in R^2,\quad a_1\rangle 0, a_2\rangle 0, b_1\in R^2, b_2\in R^2. \tag{4}$$

In particular, for image analysis, the two-dimensional digital wavelet transformation is suitable for sonar imagery decomposition [8]. The scheme of this procedure is shown in Fig. 4, where signal (image) S is divided to approximations and horizontal, vertical, and diagonal details, which are received by convolving the image with a low pass filter for approximations and with a high pass filter for details. Presented decomposition for four levels was applied for investigated

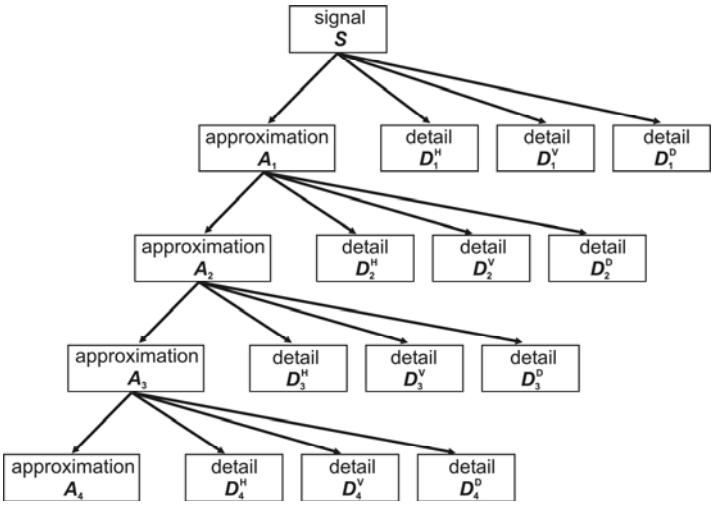

Fig.4 Multiple level wavelet decomposition tree

sonar imagery. The signal S can be presented as the sum of consecutive details and the one approximation:

$$S=\left(D_1^H,D_1^V,D_1^D\right)+\ldots+\left(D_{N-1}^H,D_{N-1}^V,D_{N-1}^D\right)+\left(A_N,D_N^H,D_N^V,D_N^D\right), \tag{5}$$

where D_N^H, D_N^V, D_N^D are horizontal, vertical, and diagonal details, N = 1,...,4 and $A_{N=4}$ is the last approximation. In applied analysis, we used biorthogonal wavelets (bior3.8), which exhibit properties of linear phase, helpful in image decomposition and reconstruction [9].

As an example of sonar image decomposition using the above method, we used the fragment of experimental area marked as a white rectangle in Fig. 3. The studied part of the seafloor is covered by ripple marks, the characteristics of which were measured using a video camera system. The main task of the described procedure was segmentation of the ripple mark area into ripples and shadows generated by ripples. Fig. 5 shows decomposition of the example image on four successive approximations, as shown in Fig. 4.

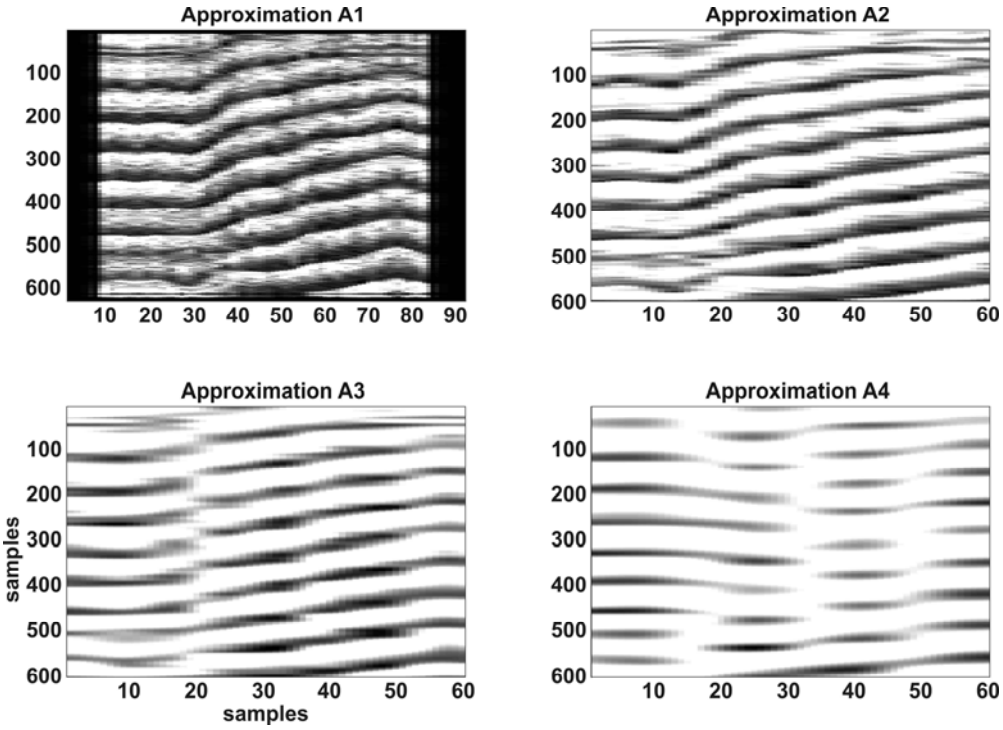

Fig.5 Decomposition of example image into successive approximations

Consecutive approximations produced using low-pass filtration are characterised by disappearing details. The best visualisation of ripple marks edges is demonstrated for the approximation of the second level (A2) and, for that reason, it was chosen as the first input to the segmentation algorithm. The next inputs were chosen from the set of wavelet decomposition details, graphical representations of which are shown in the next three figures (Figs. 6-8). In all analysed images, we can observe the disappearance of fine scale details with increasing levels of decomposition. The best results from the segmentation neural network algorithm were received for the second horizontal detail (H2), the third vertical (V3), and the third diagonal (D3) details, which, together with the approximation of the second level (A2), formed the input vector to the segmentation algorithms.

We tested two algorithms in the segmentation procedure. The first was a fuzzy c-means data clustering method (fcm). In traditional K-means clustering, each point of processed data is the member of the one cluster. Applying fuzzy logic to the clustering procedure, we can assume that the same point belongs to the different clusters with different probability.

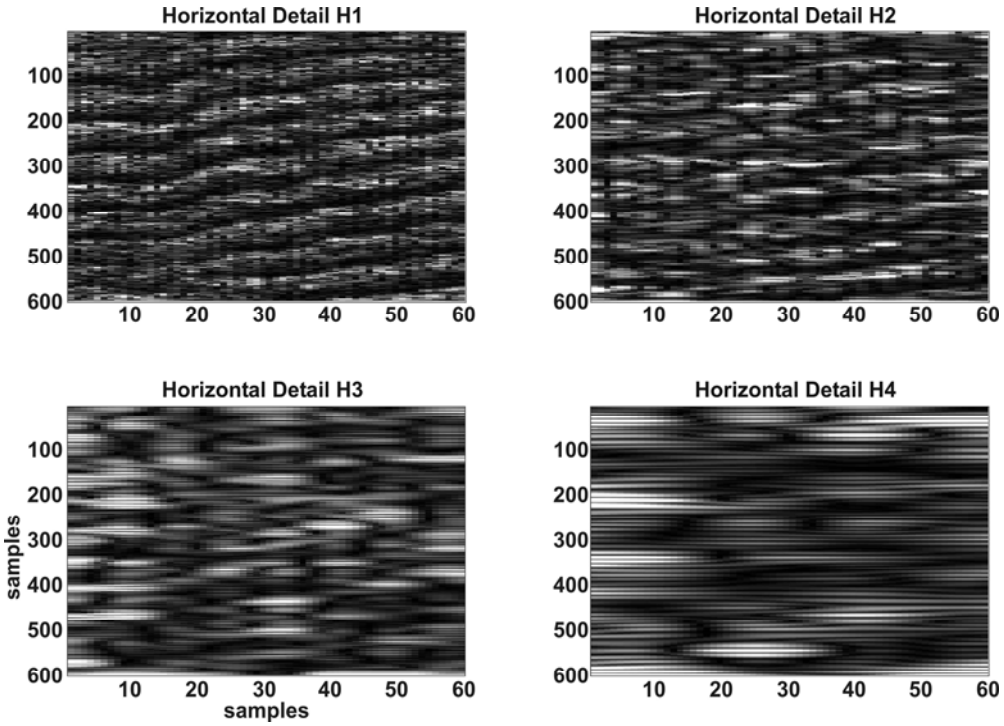

Fig.6 Decomposition of example image into successive horizontal details

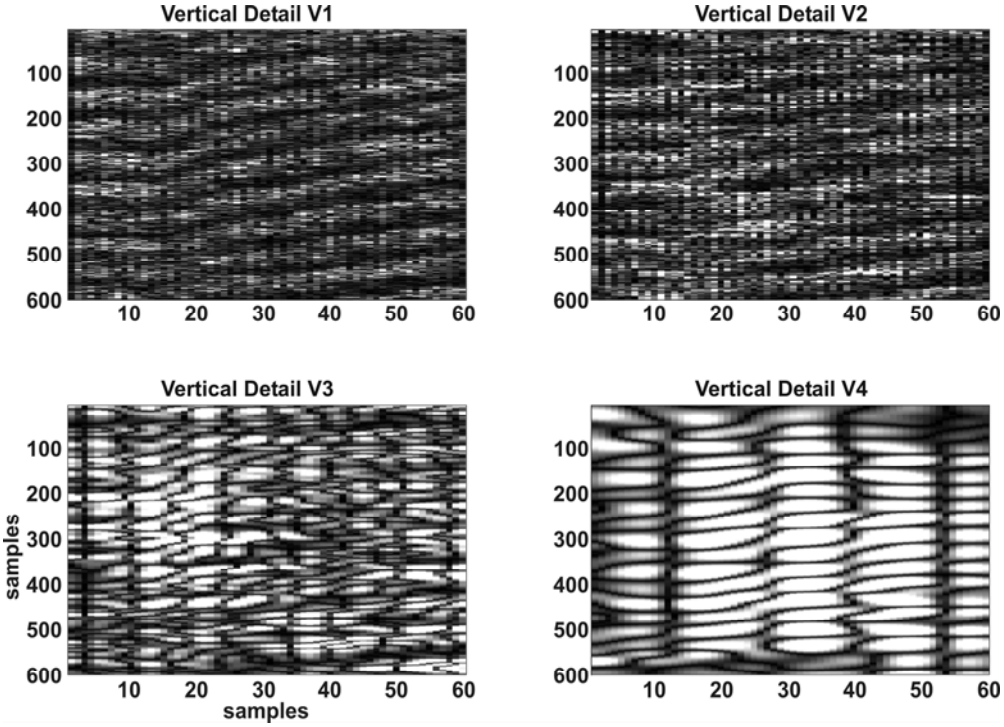

Fig.7 Decomposition of example image into successive vertical details

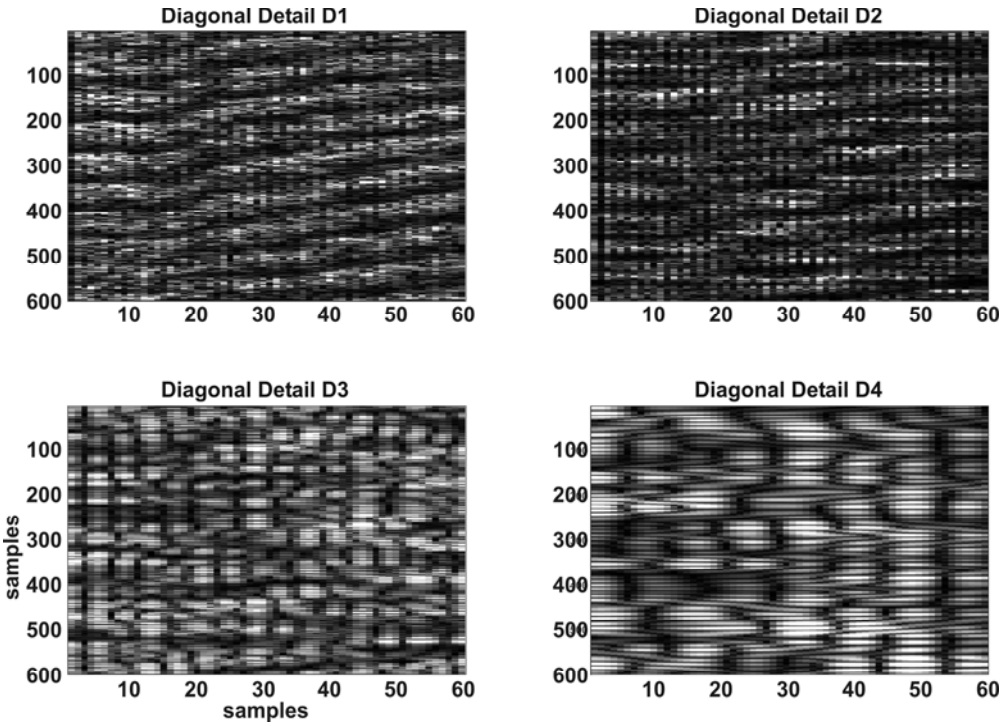

Fig.8 Decomposition of example image into successive diagonal details

In the iteration procedure, the centres of clusters and data points are moved between clusters using computation results of the minimum of the global objective function, which represents the distance of each point from the cluster centres weighted by membership grade for each cluster [10]. The result of the fcm procedure is a segmented input data set.

The other tested segmentation technique was a self-organised Kohonen's neural network [11]. This type of network is built from one-dimensional input and output layers and two-dimensional competitive layers. Each neuron from an input layer is connected with each neuron from an output layer. Input data are the object of competition, which determines the degree of neuron weight similarity to the input signal. As the result of this procedure, the "winner" neuron is identified as the neuron best fitted to the input signal. Results of both procedures were almost the same, but the computational time for the fcm algorithm was one order faster.

4. HEIGHT ESTIMATION ALGORITHM

The height estimation algorithm was constructed as follows: (i) extraction of samples belonging to shadows for each sonar image line, (ii) calculation of lengths of each shadow, (iii) assignation of shadow length to the proper ripple mark maximum, (iv) calculation of the ripple mark height based on the geometrical dependencies of measurement.

Results of the proposed algorithm were tested for real and modelled sonar imageries. Fig. 9 shows the consecutive steps of data processing. The top pictures are non processed real (a) and model (b) images. The next two images (c) and (d) are the results of a fcm segmentation procedure, which distinguished shadows from ripples. The bottom pictures (e) and (f) show results of the height estimation algorithm. The verification of algorithm correctness was made by comparison of obtained results with estimation of ripple mark heights made using scaled video recording.

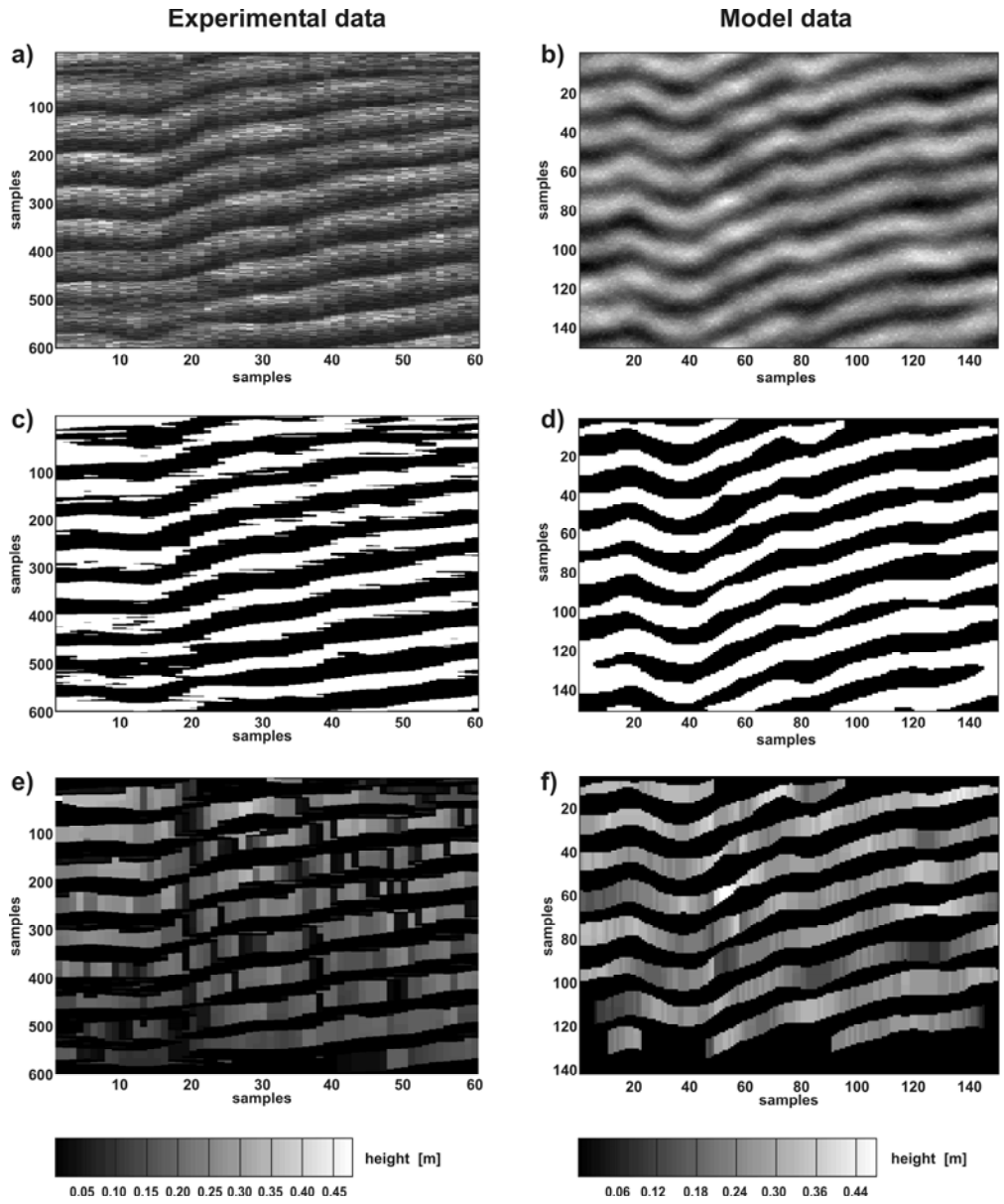

Fig.9 The ripple marks image produced by a) side-scan sonar data and b) image modelling; separation of shadows as a result of fcm segmentation procedure used for c) real data, d) model data; result of height estimation algorithm applied for e) real data and f) model data

5. CONCLUSIONS

The proposed method of seafloor irregularities height estimation gave promising results. The technique is based on a two-dimensional digital wavelet decomposition of sonar imagery inputted into a fuzzy logic clustering system or a self-organised Kohonen's neural network. The result of this procedure distinguishes shadows produced by ripple marks, obstacles, pebbles, and rocks from surroundings. Geometrical dependencies of acoustical measurement allow object height estimation. Results of the presented method are useful in Hornsund Fjord experiment data processing.

ACKNOWLEDGEMENTS

This work is supported by the Ministry of Education and Science of Poland (research project no. 2P04E 01527).

REFERENCES

[1] A. Zielinski, J. Tegowski, Acoustic Echo Formation – A Filter Theory Approach, *Proceedings of Oceans 2003 Marine Technology and Ocean Science Conference, 22-26 September 2003,* pp. 1234-1238, 2003.

[2] Ph. Blondel, B.J. Murton, *Handbook of Seafloor Sonar Imagery*, PRAXIS-Wiley, Chichester, pp. 314, 1997.

[3] R. Zhang, P. Tsai, J.E. Cryer and M. Shah, Shape form shading: a survey, *IEEE Trans. Pattern Anal. Mach. Intell*., Vol. 21, No. 8, pp. 690-705,1999.

[4] E. Dura, J. Bell and D. Lane, Reconstruction of textured seafloors from side-scan sonar images, *IEEE Proc.-Radar Sonar Navig*., Vol. 151, No. 2, pp. 114-126, 2004.

[5] S. Reed, Y. Petillot and J. Bell, Automated approach to classification of mine-like objects in sidescan sonar using highlight and shadow information, *IEEE Proc.-Radar Sonar Navig*., Vol. 151, No. 1, pp. 48-56, 2004.

[6] E. Dura, J. Bell and D. Lane, Superellipse fitting for the classification of mine-like shapes in side-scan sonar images, *Proc. MTS/IEEE Oceans, Conf. and Exhibition*, pp. 23-28, 2002.

[7] S. Reed, J. Bell, and Y. Petillot, Unsupervised segmentation of object shadow and highlight using statistical snakes, *Proc. Autonomous Underwater Vehicle and Ocean Modelling Networks: GOATS 2000, SACLANTEN Conf. Proc*. CP-46, La Spezia, Italy, pp. 221-236, 2001.

[8] S. Mallat, A theory for multiresolution signal decomposition: the wavelet representation, *IEEE Pattern Anal. and Machine Intell*., Vol. 11, No. 7, pp. 674-693, 1989.

[9] A. Cohen, I. Daubechies and J.C. Feauveau, Biorthogonal basis of compactly supported wavelets, *Comm. Pure Appli. Math.* , Vol. 45, pp. 485-560, 1992.

[10] J.C. Bezdeck, R. Ehrlich and W. Full, FCM: Fuzzy CMeans Algorithm, *Computers and Geoscience*, Vol. 10, No. 2, pp. 191-203, 1984.

[11] T. Kohonen, Adaptive, associative, and self-organizing functions in neural computing, *Appl. Opt*., Vol. 26, No. 23, pp. 4910-4918, 1987.